Sub Topic: Fire Research

9th U. S. National Combustion Meeting
Organized by the Central States Section of the Combustion Institute
May 17-20, 2015
Cincinnati, Ohio

Microgravity Flammability of PMMA Rods in Concurrent Flow

Sandra L. Olson[1], Paul V. Ferkul[2]

[1]Combustion Physics and Reacting Systems Branch, NASA Glenn Research Center at Lewis Field, m. s. 77-5, Cleveland OH, 44135-3127 USA
[2] Universities Space Research Association, Advanced Research Associates Office at NASA Glenn Research Center at Lewis Field, m. s. 110-3, Cleveland OH, 44135-3127 USA
[*]Corresponding Author Email: Sandra.Olson@NASA.gov

Abstract: Microgravity experiments burning cast PMMA cylindrical rods in axial flow have been conducted aboard the International Space Station in the Microgravity Science Glovebox (MSG) facility using the Burning and Suppression of Solids (BASS) flow duct, as part of the BASS-II experiment. Twenty-four concurrent-flow tests were performed, focusing on finding flammability limits as a function of oxygen and flow speed. The oxygen was varied by using gaseous nitrogen to vitiate the working volume of the MSG. The speed of the flow parallel to the rod was varied using a fan at the entrance to the duct. Both blowoff and quenching limits were obtained at several oxygen concentrations. Each experiment ignited the rod at the initially hemispherical stagnation tip of the rod, and allowed the flame to develop and heat the rod at a sufficient flow to sustain burning. For blowoff limit tests, the astronaut quickly turned up the flow to obtain extinction. Complementary 5.18-second Zero Gravity Facility drop tests were conducted to compare blowoff limits in short and long duration microgravity. For quenching tests, the flow was incrementally turned down and the flame allowed to stabilize at the new flow condition for at least the solid-phase response time before changing it again. Quenching was observed when the flow became sufficiently weak that the flame could no longer provide adequate heat flux to compensate for the heat losses (conduction into the rod and radiation). A surface energy balance is presented that shows the surface radiative loss exceeds the conductive loss into the rod near the limit. The flammability boundary is shown to represent a critical Damkohler number, expressed in terms of the reaction rate divided by the stretch rate. For the blowoff branch, the boundary exhibits a linear dependence on oxygen concentration and stretch rate, indicating that the temperature at blowoff must be fairly constant. For the quenching branch, the dominance of the exponential nature of the Arrhenius kinetics reaction rate indicates that the temperature is critical.

Keywords: *Flammability, Microgravity, Rod, Concurrent*

1. Introduction

NASA STD 6001 Test 1[1] is the major method used to evaluate flammability of materials intended for use in habitable environments of U.S. spacecraft. The method is an upward flame propagation test initiated in a stagnant normal gravity environment and using a well-defined igniter flame at the bottom of a vertically mounted sample. A material passes this test if the vertical burn length is less than 15.2 cm (6 inches) and there is no evidence of transfer of burning debris. The material either passes or fails the test at a given atmosphere (oxygen concentration, pressure). This test assumes that the 1g upward flame spread is conservative relative to the material's flammability in space.

What is problematic with this approach is the assumption that the 1g upward flame spread test is the worst case for flammability. Recent research has shown that current normal gravity materials flammability results are not conservative when compared to flammability in ventilated microgravity

or partial gravity conditions. Materials have sustained burning in microgravity at or below the flammability limits measured with the Test 1 protocol. What if materials are intrinsically more flammable in space than on earth, due to reduced convective cooling and yet adequate oxygen ventilation?

As part of the Burning and Suppression –II (BASS-II) experiment, twenty-four concurrent flow flammability tests with cast PMMA rods were performed in the Microgravity Science Glovebox (MSG) [2] in the Destiny Lab of the International Space Station (ISS). Twenty-two rods were clear, and two were black, but no obvious differences between clear and black have been noted to date. The objective of the BASS-II concurrent rod tests was to obtain the lower portion of the concurrent microgravity flammability map as a function of ventilation flow and ambient oxygen concentration.

Flame spread along rods with axial flow has been widely studied [3-13]. Most of the work has been downward flame spread, or opposed flow flame spread. Only a few studies have been performed in reduced gravity. Tarifa and his colleagues [9] conducted parabolic and sounding rocket opposed flow flame spread experiments with hollow rods and found that flame extinction depends considerably on both oxygen concentration and flow velocity, and quenching occurs at low flow velocities that are on the order of diffusive velocities.

Concurrent flame spread along rods was tested aboard the Mir Space Station in the Skorost hardware [14]. The extruded PMMA, Delrin, and High Density Polyethylene rods all showed the same tendency to melt beneath the flame and form accumulating molten balls on the stagnation end of the rod, with the flame wrapped around the molten ball. At low flows, the small flame at the stagnation tip of the rod propagated simply through rod regression (bulk burning) rather than through a concurrent flame spread along the rod.

Rod bulk burning via tip regression is the likely near-limit flame geometry for an axial concurrent flow along a rod in general, so we proposed to use it to study materials flammability with a simple axisymmetric geometry with minimal heat losses (surface radiation loss, conduction along the rod axis, no holder losses). The heat loss can be varied by varying the diameter of the rod, which effectively changes the surface energy balance term associated with in-depth conduction from the surface.

2. Experimental Setup

The BASS-II hardware used for these tests is shown inside the MSG working volume in Figure 1. The BASS-II hardware consists of a flow duct, still camera, video camera, external control box and associated plumbing and mounting systems. The three primary variables included the working volume oxygen concentration, the flow velocity through the duct, and the PMMA rod diameter.

The black anodized 7.6 cm x 7.6 cm x 17 cm rectangular flow duct with rounded corners was originally built to perform gas jet diffusion flame studies [15], and was modified to accommodate solid samples for the BASS series of experiments. The flow through the duct was generated using a small fan at the upstream end of the duct. The voltage to the fan was varied to change the flow through the duct. In addition, up to two additional flow restrictors could be used at the fan inlet to increase the pressure drop and thus reduce the flow through the duct to the desired value for the test point. The flow then passed through a honeycomb flow straightener and an inlet screen to reduce swirl. An omnidirectional spherical air velocity transducer (TSI™ # 8475) was positioned between the honeycomb and the screen, and was used to measure the steady-state flow velocity through the duct. The air velocity transducer probe had a response time of approximately one minute. The fan voltage

TM Mention of trade names or commercial products is for descriptive purposes only and does not constitute endorsement or recommendation for use by the U.S. Government.

was calibrated with the air velocity transducer reading at the end of every operations day using that day's flow restrictor configuration(s).

The test section was 17 cm long. Inside the test section was a nozzle for nitrogen flow to vitiate the working volume, a moveable scale to provide a reference at the sample plane, and an Oriel™ #71768 thermopile detector with a Calcium Fluoride window with a spectral range of 0.13 to 11 microns in the downstream top back corner of the duct. The test section of the duct had two orthogonal windows, the top one being replaced for BASS to provide a mounting rail system for the solid samples. The top window was used by a Nikon™ D300 12.3 megapixel digital color still camera with a 60 mm lens that provided 4320 x 2968 pixel images. The duct exit contained a perforated copper plate followed by a brass screen to provide heat rejection and a cold surface for soot deposition. The flow turned ninety degrees to exit the duct, which facilitated mixing of the hot combustion gases with the cool ambient air.

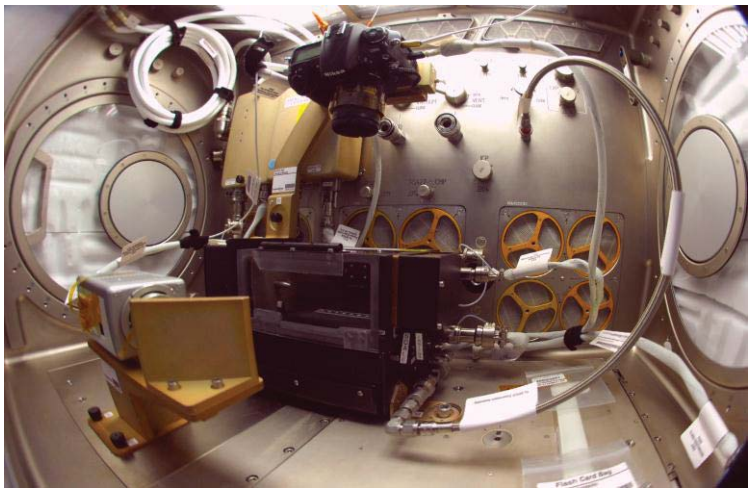

Figure 1. Microgravity Science Glovebox Facility (MSG) working volume aboard the International Space Station (ISS) with the Suppression of Solids – II (BASS-II) experiment hardware installed.

The front window opened to provide access to the test section for sample and igniter change out. A Panasonic color video camera WV-CP654 (760 x 480 pixel array) with a turning mirror looked in the front window. The video camera had a built-in digital overlay that displayed the nitrogen flow rate (cm^3/min), fan voltage (10xV), hot wire anemometer reading (cm/s), and the radiometer signal. The radiometer signal was not calibrated, but provided a measure of the flame dynamics and steadiness. The external control box had controls for the fan voltage level, nitrogen flow level, enable switches for the igniter and nitrogen, and a radiometer gain level setting.

Seventeen clear cast PMMA cylindrical rods of various diameters (11with 1/4", 4 with 3/8", and 2 with 1/2" diameters) were burned in a concurrent flow direction. The samples were manually ignited by the astronaut at the initially hemispherical stagnation tip with a Kanthal™ A-1 29 gauge hot-wire igniter with a nominal hot wire resistance of 0.8-1 ohms, powered by approximately 3.5-3.8 amps. Samples are burned within the duct and the combustion products exit the duct and mix with the gas in the work volume.

To evaluate the levels of combustion products produced during microgravity fires, we used on-board sensors to measure the O_2 depletion and the completeness of combustion (CO, CO_2). The O_2, CO_2, and CO measurements required two portable, battery powered instruments in the working volume during testing: CDM, and CSA-CP. The oxygen sensor is not recalibrated on orbit, so we also used

the Mass Constituents Analyzer data to determine the oxygen sensor offset on a daily basis. The resolution of the CSA-CO was 0.1% O_2. Oxygen concentrations in the MSG working volume were varied during the testing from ambient ISS oxygen levels (~ 21% O_2) down to ~14% O_2 for very near-limit flames. The CO sensor is zero calibrated every 60 days, with a range of 0-1000 ppm and a resolution of 1 ppm. The CO_2 sensor was within its calibration window, and had a range of 0-5% and a resolution of 0.1% by volume of CO_2. The sensor data provided initial and final conditions for repeated tests in a sealed working volume, and allowed us to determine when the working volume needed to be purged.

To obtain the desired vitiated atmosphere, the MSG working volume was diluted using ISS nitrogen (hose connecting BASS-II duct to back wall of MSG in Figure 1). The nitrogen was regulated with a small (< 0.5 LPM) MKS™ 179A mass flow meter and entered the flow duct through a small nozzle just downstream of the fan in the test section. The fan in the flow duct was turned to maximum (> 100 LPM) during the nitrogen flow to mix and blow the gas into the working volume and circulate it continuously throughout the hours-long vitiation. We developed a vitiation model [16] based on a Continuously Stirred Tank Reactor (CSTR) model. This perfect mixing approximation is valid as long as the residence time (V/r = 500 min) is 5 to 10 times as long as the mixing time, which is easily the case for the 100 LPM mixing rate (250 L/100 LPM = 2.5 min mixing time). The model was verified using intermittent on-board oxygen sensor readings during an initial vitiation. This model was then used to determine the nitrogen flow rate and flow time to achieve the desired oxygen concentration of the test based upon the initial oxygen concentration reading and operational crew time constraints.

3. Results and Discussion

To start each experiment, the astronaut ignited the rod at the stagnation tip and allowed the flame to develop and heat the rod axially at a sufficient flow to sustain burning. The time needed to adequately develop the solid-phase thermal profile is estimated to be when the Fourier number is approximately equal to 0.3 ($Fo= \alpha t/R^2 \sim 0.3$) [17]. For a thermal diffusivity of PMMA=1.2×10^{-3} cm^2/s, the times range from 25 s to 100 s for the different rod radii tested.

3.1 Quenching Extinction

For quenching tests, the flow was incrementally turned down and the flame allowed to stabilize at the new flow condition for at least the solid-phase response time before changing it again. Quenching was observed when the levels of forced flow and/or oxygen concentration became sufficiently weak that the flame could no longer provide adequate heat flux to compensate for the heat losses (conduction into the rod and radiation). Quench test burns lasted up to 28 minutes. Near –quenching flames for each rod size are shown in Figure 2.

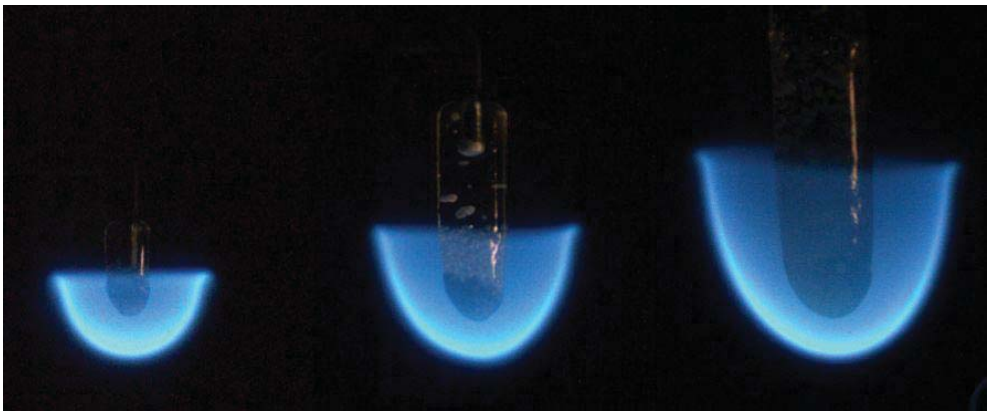

Figure 2: Representative near-limit flames for each of the three rod sizes tested: left to right R= 1/8” (0.318 cm), 3/16” (0.476 cm), and ¼” (0.635 cm). Flow and oxygen are not the same, but each represents the lowest oxygen test for that rod size.

3.1 Blowoff extinction

For blowoff limit tests, the astronaut quickly turned up the flow to obtain extinction. The flow at blowoff was defined by the fan voltage reading at the moment the stagnation region opened up and the flame moved downstream. The annular flame would oscillate upstream and downstream multiple times before completely blowing off. Later in the test program, we attempted to re-establish the stagnation region after local blowoff by quickly reducing the flow to a value below the blowoff velocity, but we were only successful in one instance where the blowoff of the stagnation region may not have been complete (flame opening less than a thermal length, perhaps) due to the astronaut's quick response time. A subsequent attempt shortly after this was not able to re-establish the stagnation region, so it seems that once the flame is blown downstream of the stagnation region, the flame is unable to propagate upstream for the low oxygen levels tested (16.1% O_2 and lower). This is consistent with tests for opposed flow flame spread rods that were also done as part of BASS-II [18], where flame spread was not observed below 16.4 % O_2. Example blowoff images are shown in Figure 3.

3.2 Drop Tower tests

Complementary 5.18-second Zero Gravity Facility drop tests were conducted to compare blowoff limits in short and long duration microgravity, using the microgravity wind tunnel drop rig [19]. For the drop tests, the rod was ignited in normal gravity and allowed to burn and preheat the rod briefly at a flammable oxygen flow, and then the gas was switched to the test atmosphere and the package released based on the flow time of the gas to reach the flame zone. The flames in the drop tower blowoff tests are significantly smaller than the ISS flames, as can be seen in Figure 3. This is most likely due to the short burn time prior to blowoff, so the rod was not significantly preheated.

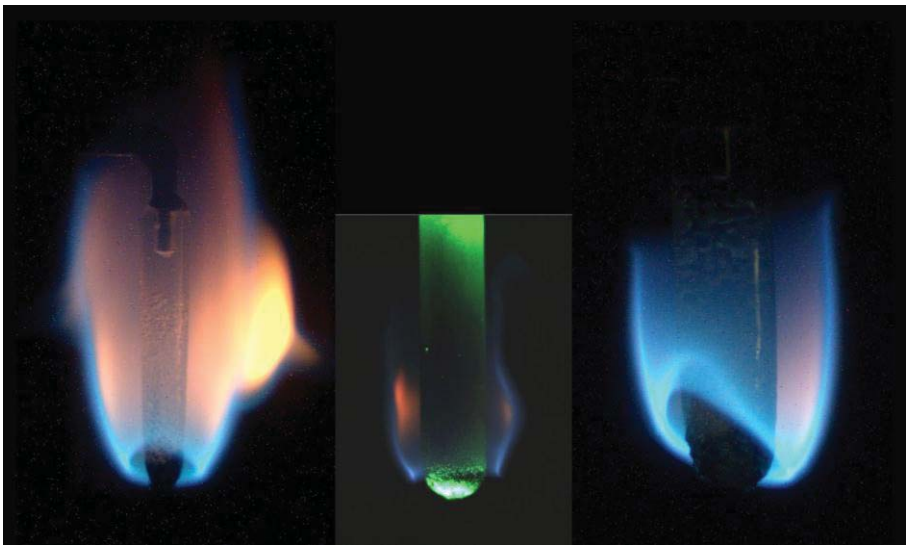

Figure 3: Blowoff images for three rod sizes: left to right R= 1/8" (0.318 cm), 3/16" (0.476 cm), and ¼" (0.635 cm). Center image is of a 5.18-second Zero Gravity Research Center drop test, where the flame blew off during the drop, since no ISS blowoff tests were obtained with the intermediate rod size. A green LED illuminates the drop test rod. Flow and oxygen are not the same, but each represents the lowest oxygen test for that rod size.

3.4 Flammability Boundary

For each test, the flow at which the flames extinguished and the last flow where a stable flame was observed (or where the flame did not blowout in the drop time for drop tests), along with the post-burn oxygen reading were used to generate the flammability boundary, shown in Figure 4. There appears to be a different O_2 minimum for the 0.476 cm and 0.635 cm radius rods, which is attributed to increased solid conductive heat loss for the larger rod cross sectional area.

The thick gray flammability boundary is the border between stable flames and extinguished flames. It is a stochastic region due to the fact that near the flammability boundary, the flame is sensitive to perturbations, and a random perturbation of sufficient magnitude will extinguish a flame in this near-limit region [20]. The gray stochastic boundary is defined by the combined equations shown by the red and black dashed lines. These dashed lines are based on a critical Damkohler number analysis, where a critical Damkohler number (Da_{crit}) is defined as

$$Da_{crit} = \left[\frac{flow\ time}{reaction\ time}\right]_{crit} \sim \left[\frac{reaction\ rate}{flow\ rate}\right]_{crit}$$

$$\sim \left[\frac{A_g\,(\rho_g Y_f)(\rho_g Y_{ox})e^{(-E_g/RT_g)}}{a}\right]_{crit}$$

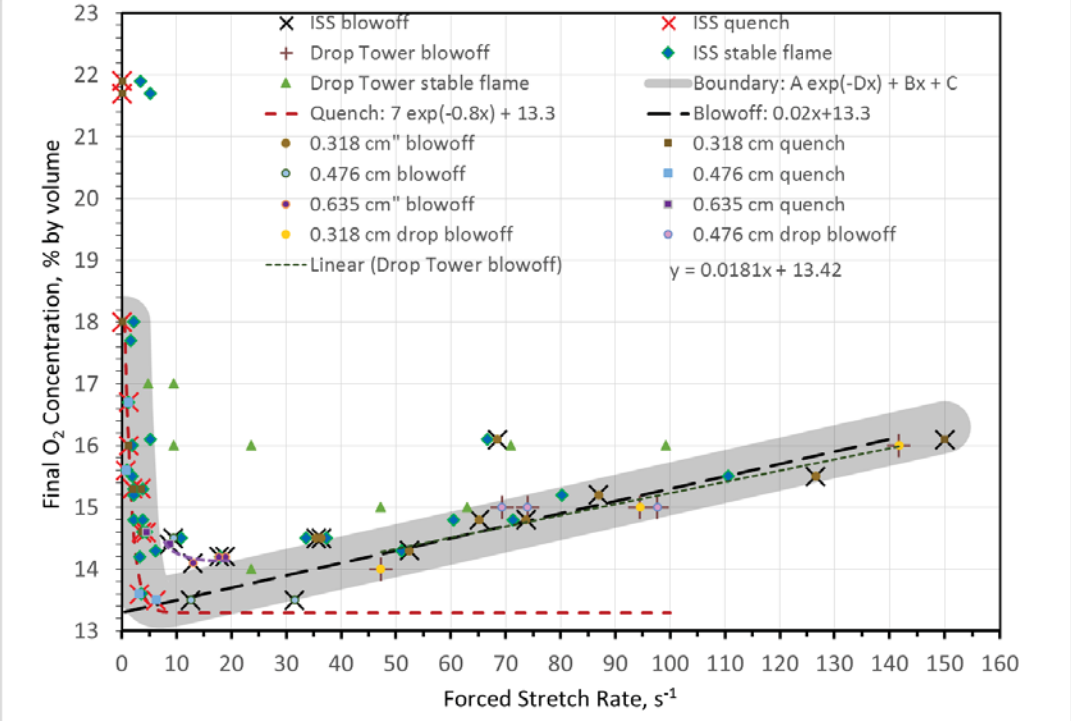

Figure 4: Flammability boundary obtained in BASS-II tests with concurrent rods of different sizes. Complementary drop tower test results are also shown. Extinction points (X's) are color-coded to indicate rod diameter.

Notice that the black dashed line blowoff boundary in Figure 4 is linear ($Y_{ox} \sim a$), which would seem to indicate that the dominant parameters for blowoff are these parameters in the Da_{crit} equation. This implies that the fuel concentration and the critical temperature are fairly constant in the flame zone at blowoff where the reactants move so quickly through the reaction zone that they do not have

time to react. The critical temperature for ignition is a well-known concept that can be applied to blowoff if one considers the fuel and oxidizer to be in a state of continual ignition in the flame zone. Once the temperature in the flame zone drops below the critical temperature for ignition, the flame blows off.

The drop tower blowoff data linear curve fit is plotted for comparison, and agrees very well with the ISS data. This further implies that the different levels of preheating of the rod do not affect blowoff extinction. The linear blowoff boundary has interesting implications in that it may be possible to linearly extrapolate blowoff data down to zero stretch rate and use that oxygen value as a conservative estimate of the minimum oxygen concentration where the material will burn. This will allow us to de-rate materials based on normal gravity flammability tests to ensure the material will not burn in space. Using the y-intercept of the linear fit (13.3 % O_2 in the Figure 4 fit, versus the minimum test point of 13.6 % O_2) would add a slight level of conservatism.

On the other hand, the quenching branch is captured with a red dashed exponential fit. This suggests the Arrhenius temperature exponential term is dominant in the quenching region. This is expected at quenching, where the temperature drops off dramatically while flow time is plentiful. Heat losses dominate to cool the flame to extinction, as was modeled by [20, 21]. This boundary is very steep when plotted on a linear x axis as shown in Figure 4. To get the "U"-shaped flammability boundary, a logarithmic x axis is often used, which expands the quenching branch while making the linear blowoff branch have a curved shape.

We recognize that the appropriate flow parameter to use to compare data for the different rod sizes is the flame stretch, which is defined here as sum of the combined flow-induced stretch and the curvature-induced stretch, or $a=a_f + a_{curv}$. The effect of curvature-induced stretch is not negligible for these small diameter rods at low speed flows, and we combine them in this way following the example for mixed convection [21]. The initial rod tip is hemispherical, but as it burns it takes on a slightly more tapered round-nosed shape, as can be seen in Figures 2 and 3. The flow-induced stretch around the approximately spherical rod tip is $a_f = 3/2$ U/R. The curvature-induced stretch around the hemispherical flames is estimated for the small samples as $a_{curv} = [3\ U/R] \times [(R_{flame}-R)/R]$.

The analysis of all the data for flame radius at each limit condition is not yet complete, so Figure 4 currently shows the flammability boundary data plotted as forced stretch rate, with the data points also marked by rod size. The data points will shift to the right once the curvature-induced stretch is accounted for. Table 1 gives estimates of the curvature-induced stretch for each radius, based on the flame radii measured from Figure 2, to give an idea of the magnitude of the shift.

Table 1: Stretch rate estimates for specific tests shown in Figure 2

Rod radius, cm	a_f = 3/2 U/R, s^{-1}	$a_{curv} = [3\ U/R] \times [(R_{flame}-R)/R]$, s^{-1}	$a=a_f + a_{curv}$, s^{-1}
0.318	2.36	3.63	5.99
0.476	3.46	4.62	8.08
0.635	3.31	5.38	8.68

3.5 Surface Energy Balance

If we assume for long burn times that the solid phase thermal profile away from the flame tip has reached an approximate steady state, we can approximate the 1D temperature profile along the rod axis.

Away from the regressing tip of the rod, there is a balance of heat transfer through the rod via conduction and convection:

$$0 = \rho_s c_s V_r \frac{\partial T_s}{\partial y} + \lambda_s \frac{\partial^2 T_s}{\partial y^2}$$

The convective term is due to the steady surface regression of the rod (measured from the experiment), V_r. It is assumed in this steady analysis that V_r is so small that the length of the sample does not change significantly over the timeframe of interest τ, over which $\Delta L \ll L$, where L is the characteristic length of the rod. This means that changes in the temperature profiles are quasi-steady for a slowly changing L.

Boundary conditions include the surface temperature at y=0 is T_s (assumed a constant pyrolysis temperature) and the ambient temperature at y = L is T_∞. Non-dimensionalizing with $Y=y/L$, $\theta = (T-T_\infty)/(T_s-T_\infty)$, and $Pe= LV_r/\alpha_s$ we can write

$$0 = Pe \frac{\partial \theta_s}{\partial Y} + \frac{\partial^2 \theta_s}{\partial Y^2}$$

The coefficient is a solid-phase Peclet number, which is a ratio of the convective heat transferred as the fuel regresses, compared to the conductive heat transfer from the hot surface. Boundary conditions become $\theta(0)=1$ and $\theta(1)=0$. This equation is a linear, homogeneous, second order ordinary differential equation with constant coefficients, with roots 0 and -Pe for a *general* solution

$$\theta(Y) = C_1 e^{-PeY} + C_2 e^0$$

Using the boundary conditions to evaluate C_1 and C_2, we find the solution is

$$\theta(Y) = \frac{\exp(-PeY) - \exp(-Pe)}{1 - \exp(-Pe)}$$

For large Peclet numbers (Pe>1), there is a substantial change in the non-dimensional gradient due to the increasing exponential nature of the temperature profiles, since heat conducted along the rod is convected back toward the burning tip so that heat cannot penetrate too deeply along the rod. For small Peclet numbers (Pe≤1), conduction dominates and the temperature profiles are nearly linear. It is counter-intuitive that the slowest burning samples will, in this steady-state, have the least heat loss into the solid, which has been previously noted [23].

We can differentiate the 1D solution to evaluate the steady-state temperature gradient at the regressing surface (Y=0) with decreasing Peclet number (burning rate). Solving for the temperature gradient at the surface as a function of Peclet number, we obtain

$$\frac{d\theta}{dY}\Big|_{Y=0} = \frac{Pe}{\exp(-Pe) - 1}$$

We can use this to evaluate the conductive loss down the rod as a function of regression rate (Pe), and estimate the flame heat flux as a function of Peclet number.

The surface energy balance for the rod tip is given by

$$q''_{flame} = \lambda_g \frac{\partial T_g}{\partial x}\Big|_s + q''_{rad} = \lambda_s \frac{\partial T_{solid}}{\partial x}\Big|_s + \dot{m}'' L_{vap} + \varepsilon\sigma(T_s^4 - T_\infty^4)$$

Where L_{vap} = 1700 J/g, m" = $V_r\rho$, ε = 0.85, T_s = 300 °C, λ_s = 2.09 x 10^{-3} W/cm K at 300 K, λ_g = 5.77 x 10^{-4} W/cm K at 800 K, ρ = 1.19 g/cc, L=5.9 cm, and σ = 5.729 x 10^{-12} W/cm^2 K^4

Using these values and evaluating the surface temperature gradient as above, we can estimate each term in the energy equation as a function of the Peclet number in Figure 5. It has been shown [17] that the burning rate decreases nearly linearly with stretch rate until very near the quenching or blowoff limits, so Pe ~ a. As mentioned above, solid conduction decreases with decreasing Peclet number. Surface radiative loss is assumed to be constant. The energy available for fuel vaporization decreases with decreasing Peclet number, as one would expect. The net flame heat flux thus drops precipitously with decreasing Peclet number.

We can compare the importance of the different losses by normalizing them with the net flame heat flux (left side of energy balance, which includes gas-phase conduction and gas radiation). In Figure 5, the solid conduction, surface radiation, and the combined solid conduction and surface radiative loss are normalized by the net flame heat flux and are plotted on the right axis. As Peclet number decreases (rod regression rate decreases as forced stretch rate decreases), the radiative loss ratio increases dramatically since surface radiative loss is a constant while flame heat flux decreases linearly with Peclet number. The solid conduction ratio actually falls off as Peclet number is reduced. The combined radiative and conductive loss ratio increases at low Peclet number, and one would expect the flame to quench when the combined losses exceed approximately 70% of the net flame heat flux [24, 25]. The primary reason for quenching is the reduced net heat flux from the flame compared to the ongoing losses.

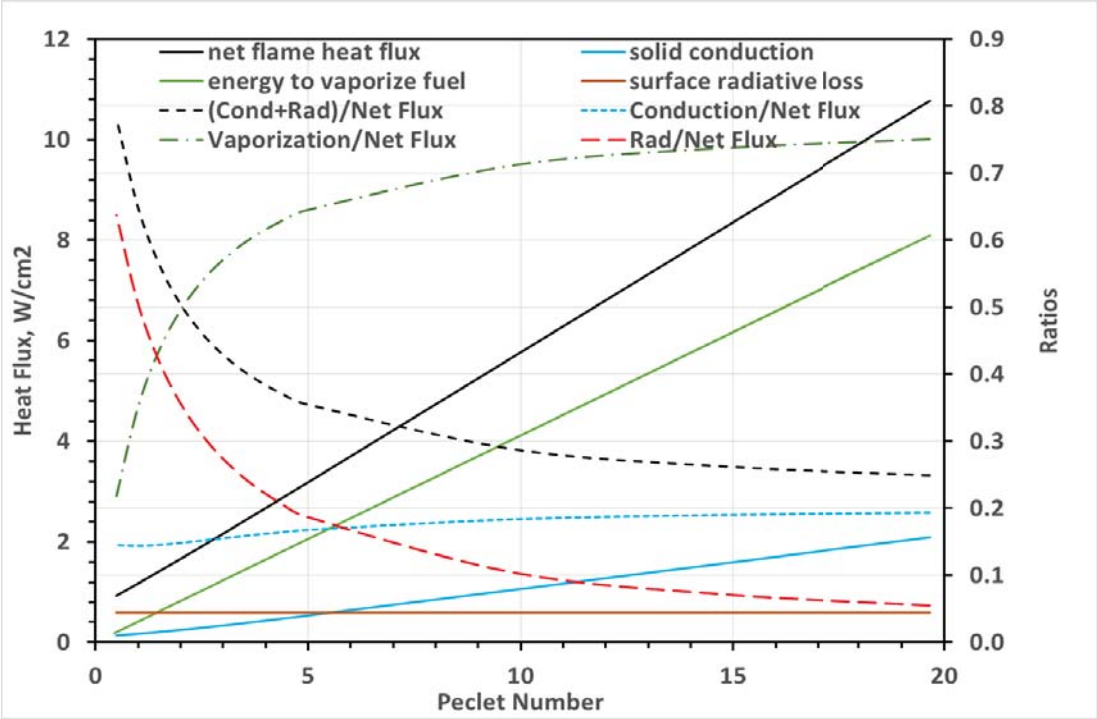

Figure 5: Surface Energy Balance terms. As the rod regression rate decreases (Pe decreases, *a* decreases), the relative importance of heat losses increases, eventually causing quenching. At quenching, surface radiation is higher than solid conduction loss, but the primary reason for quenching is the reduced net heat flux from the flame compared to the ongoing losses.

4. Conclusions

Twenty-four concurrent axial flow flammability tests with three diameters of cast PMMA cylindrical rods were performed in the MSG on the ISS. Oxygen concentrations in the MSG working volume were varied during the testing from ambient ISS oxygen levels (~ 21% O_2) down to ~14% O_2, and oxygen concentrations before and after each test were measured with an on-board CSA-CP sensor. Flow velocity through the duct was also varied by changing the fan voltage, and measured with a hot-wire anemometer.

In quenching limit tests, the flow was incrementally turned down and the flame allowed to stabilize at the new flow condition for at least the solid-phase response time before changing it again. For blowoff limit tests, the astronaut quickly turned up the flow to obtain extinction. Complementary 5.18 second Zero Gravity Facility drop tests were conducted to compare blowoff limits in short and long duration microgravity.

A flammability boundary with axes of oxygen concentration and forced stretch rate is obtained that has a distinctive shape that correlates well with a critical Damkohler number. The blowoff branch exhibits a linear ($Y_{ox} \sim a$), trend that indicates there is a relatively constant critical temperature at blowoff. The quenching branch exhibits an exponential (Y_{ox} versus a) curve which reflects importance of heat losses to drop the flame temperature, causing the Arrhenius reaction rate to slow to a critical Damkohler number while flow time is plentiful. A surface energy balance is used to show how the reductions in net flame heat flux at low stretch (low regression rates) drives the flame to quenching extinction despite the fact that the losses actually decrease slightly near the limit.

5. Acknowledgements

This work was funded by the ISS Research Project Office. We want to acknowledge the invaluable assistance of astronauts Don Pettit, Reid Wiseman and Alex Gerst, who ran the BASS experiments reported here. This work couldn't have been done without the intense efforts of the BASS ops team (Jay Owens, Chuck Bunnell, Tibor Lorik, and Carol Reynolds). We also want to acknowledge the ground support teams at GRC, JSC, and MSFC that supported the BASS-II operations.

6. References

1 NASA STD-6001B, 2011.
2 R. A. Spivey, W. A. Sheredy, and G. Flores, 46th AIAA Aerospace Sciences Meeting and Exhibit, 7 - 10 January 2008, Reno, Nevada, AIAA-2008-812.
3 J. De Ris, A. M. Kanury, and M. C. Yuen, Proc. Comb. Inst. 14 (1973) 1033-1044.
4 M. Sibulkin, and C.K. Lee, Comb. Sci. Tech. 9, (1974)137-147.
5 A. C. Fernandez-Pello, and R. J. Santoro, Proc. Comb. Inst. 17 (1979) 1201-1209.
6 Fernandez-Pello, A. C., Ray, S. R., and Glassman, I., Combust. Sci. Tech. 19 (1978) 19-30.
7 S. R. Ray, Dissertation, Princeton University, 1982.
8 Y. Halli, J. S. T'ien, NBS-GCR-86-507 (1986).
9 C. S. Tarifa, B. Lazaro, First Int'l. Symp. on Microgravity Research and Applications on Physical Sciences and Biotechnology, 2000.
10 R. O. Weber, and N. J. de Mestre, Comb. Sci. Tech. 70 (1990) 17-32.
11 M.A. Delichatsios, Proc. Comb. Inst. 28 (2000) 2899-2904.
12 M.A. Delichatsios, R.A. Altenkirch, M.F. Bundy, S. Bhattacharjee, L. Tang, and K. Sacksteder, Proc. Comb. Inst. 28 (2000) 2835–2842.
13 F. J. Higuera, Comb. Theory & Modelling 6 (2002) 197-208.
14 A.V. Ivanov, Ye.V. Balashov, T.V. Andreeva, A.S. Melikhov, NASA–CR–1999–209405 (1999).
15 K.T. Dotson, P.B. Sunderland, Z.G. Yuan, and D.L.Urban, Fire Safety J. 46 (2011) 550-555.
16 S. L. Olson, P. V. Ferkul, S. Bhattacharjee, F. J. Miller, A. C. Fernandez-Pello, S. Link, and J. S. T'ien, ICES-2015-196, 45th International Conference on Environmental Systems, 12-16 July 2015, Bellevue, Washington.
17 S. L. Olson, Case Western Reserve University Dissertation, May, 1997.
18 S. Link, C. Fernandez-Pello, S. Olson, P. Ferkul, 30th annual meeting of the American Society for Gravitational and Space Research (ASGSR), Pasadena, CA, Oct. 23-26, 2014.
19 S. L. Olson, Combustion Science and Technology, 76 (1991) 233-249.
20 J. S. T'ien, Combust. Sci. Tech. 7 (1973), 185-188.
21 D. W. Foutch and J. S. T'ien, AIAA J. 25 (7), (1986), 972-976.
22 T'ien, J. S., Combust. Flame, Vol. 65 (1986) 31-34.
23 Ohtani, H., Akita, K., and Hirano, T., *J. Fire Flammability* 13 (1982) 203–214.
24 S.L. Olson, T Kashiwagi, O. Fujita, M. Kikuchi, and K. Ito, Combust. Flame 125 (2001) 852-864.
25 J. B. Armstrong, S. L. Olson, and J. S. T'ien, Combust. Flame147 (2006) 262-277.